J|A|C|S
ARTICLES
Published on Web 04/01/2004

Chemoselective Hydrogenation Catalysts: Pt on Mesostructured CeO_2 Nanoparticles Embedded within Ultrathin Layers of SiO_2 Binder

Patricia Concepción,[†] Avelino Corma,*,[†] Joaquín Silvestre-Albero,[†] Victor Franco,[‡] and Jean Y. Chane-Ching[§]

Contribution from the Instituto de Tecnología Química, UPV-CSIC, Universidad Politécnica de Valencia, Av. de los Naranjos s/n, 46022 Valencia, Spain, Departament de Física Fonamental, Universitat de Barcelona, Spain, and Rhodia Recherches, 52 Rue de la Haie Coq, 93 308 Aubervilliers, France

Received December 17, 2003; E-mail: acorma@itq.upv.es

Abstract: Pt on mesostructured CeO_2 nanoparticles embedded within ultrathin layers of highly structured SiO_2 binder shows highest activity reported with 80% selectivity for the chemoselective hydrogenation of crotonaldehyde. Characterization by transmission electron microscopy (TEM), CO adsorption, and X-ray photoelectron spectroscopy (XPS) show the presence of small Pt metal particles, preferentially located on CeO_2 (70%) together with the formation of Pt−CeO_{2-x} sites at the interface between Pt and CeO_2 (4 nm) nanoparticles. These sites are able to polarize the carbonyl group and facilitate the selective hydrogenation of this with respect to the double bond.

Introduction

The search for chemoselective catalysts is an issue of great interest for the production of many pharmaceutical, agrochemical, and fragrance compounds.[1−3] In this sense, the selective hydrogenation of the carbonyl bond in α,β-unsaturated aldehydes by use of metal catalysts is still an unsolved problem in heterogeneous catalysis. Selective reduction can be achieved by means of properly designed organometallic catalysts,[4] through a Merwein-Pondorf reaction with alcohols as reducing agents and solid Lewis acids as catalysts.[5−7] Good selectivities can also be achieved by means of sulfur-modified Cu/Al_2O_3[8] or gold catalysts.[9] However, the use of monometallic platinum catalysts and H_2 leads mainly to the formation of the saturated aldehyde, which is thermodynamically and kinetically the most favored product.[10] Therefore, a promotion of the metal is necessary in order to increase the selectivity toward the formation of the unsaturated alcohol. The promotion could involve either the C=O double-bond polarization and/or the inhibition of the α,β-unsaturated aldehyde adsorption through the C=C bond.[1] This promotion can be achieved by the addition of a second, more electropositive metal like iron[11] or tin[12,13] or by the use of oxide supports such as CeO_2,[14−18] TiO_2,[19,20] ZnO,[21] MgO,[22] or SnO_2,[23] which are able to interact with the platinum. The presence of electronic effects and/or alloy formation, together with the induction of strong metal−support interactions (SMSI) when partially reducible oxides are used as a support, have been proposed to be responsible for the improved selectivity. In this sense, cerium-based platinum catalysts have been extensively studied for the selective hydrogenation of an α,β-unsaturated aldehyde, such as crotonaldehyde. It has been reported that platinum promotion by ceria enhances the selectivity toward the hydrogenation of the carbonyl bond,[14−18] either by the creation of defect sites at the metal−oxide interface after

[†] Universidad Politécnica de Valencia.
[‡] Universitat de Barcelona.
[§] Rhodia Recherches.

(1) Gallezot, P.; Richard, D. *Catal. Rev.—Sci. Eng.* **1998**, *40*, 81.
(2) Corma, A.; Nemeth, L. T.; Renz, M.; Valencia, S. *Nature* **2001**, *412*, 423.
(3) De Bruyn, M.; Coman, S.; Bota, R.; Parvulescu, V. I.; De Vos, D.; Jacobs, P. A. *Angew. Chem., Int. Ed.* **2003**, *42*, 5333.
(4) Ohkuma, T.; Ooka, H.; Ikariya, T.; Noyori, R. *J. Am. Chem. Soc.* **1995**, *117*, 10417.
(5) Corma, A.; Garcia, H. *Chem. Rev.* **2003**, *103*, 4307.
(6) Corma, A.; Domine, M. E.; Nemeth, L.; Valencia, S. *J. Am. Chem. Soc.* **2002**, *124*, 3194.
(7) Corma, A.; Domine, M. E.; Valencia, S. *J. Catal.* **2003**, *215*, 294.
(8) Hutchings, G. J.; King, F.; Okoye, I. P.; Padley, M. B.; Rochester, C. H. *J. Catal.* **1994**, *148*, 464.
(9) (a) Bailie, J. E.; Hutchings, G. J. *Chem. Commun.* **1999**, 2151. (b) Bailie, J. E.; Abdullah, H. A.; Anderson, J. A.; Rochester, C. H.; Richardson, N. V.; Hodge, N.; Zhang, J. G.; Burrows, A.; Kiely, C. J.; Hutchings, G. J. *Phys. Chem. Chem. Phys.* **2001**, *3*, 4113.
(10) Giroir-Fendler, A.; Richard, D.; Gallezot, P. *Stud. Surf. Sci. Catal.* **1988**, *41*, 171.
(11) Marinelli, T. B. L. W.; Nabuurs, S.; Ponec, V. *J. Catal.* **1995**, *151*, 431.
(12) Coloma, F.; Sepúlveda-Escribano, A.; Fierro, J. L. G.; Rodríguez-Reinoso, F. *Appl. Catal. A* **1996**, *148*, 63.
(13) Margitfalvi, J. L.; Vankó, Gy.; Borbáth, I.; Tompos, A.; Vértes, A. *J. Catal.* **2000**, *190*, 474.
(14) Sepúlveda-Escribano, A.; Coloma, F.; Rodríguez-Reinoso, F. *J. Catal.* **1998**, *178*, 649.
(15) Abid, M.; Touroude, R. *Catal. Lett.* **2000**, *69*, 139.
(16) Silvestre-Albero, J.; Rodríguez-Reinoso, F.; Sepúlveda-Escribano, A. *J. Catal.* **2002**, *210*, 127.
(17) Sepúlveda-Escribano, A.; Silvestre-Albero, J.; Coloma, F.; Rodríguez-Reinoso, F. *Stud. Surf. Sci. Catal.* **2000**, *130*, 1013.
(18) Abid, M.; Touroude, R. *Catal. Lett.* **2000**, *69*, 139.
(19) Dandekar, A.; Vannice, M. A. *J. Catal.* **1999**, *183*, 344.
(20) Vannice, M. A. *Top. Catal.* **1997**, *4*, 241.
(21) Consonni, M.; Jokic, D.; Murzin, D. Y.; Touroude, R. *J. Catal.* **1999**, *188*, 165.
(22) Homs, N.; Llorca, J.; Ramirez de la Piscina, P.; Rodríguez-Reinoso, F.; Sepúlveda-Escribano, A.; Silvestre-Albero, J. *Phys. Chem. Chem. Phys.* **2001**, *3*, 1782.
(23) Liberková, K.; Touroude, R. *J. Mol. Catal.* **2002**, *180*, 221.

a high-temperature reduction treatment (773 K), which are able to activate the C=O double bond, or by electronic effects on platinum that may even form Ce−Pt alloy phases upon a reduction treatment at high temperature (973−1173 K).[15,24]

All the above potential positive effects of CeO_2 on the preparation of chemoselective Pt-supported catalysts should be enhanced if one were able to prepare high surface area, well-structured CeO_2 supports. Here, we present a new CeO_2-derived material formed by nanocrystals of CeO_2 with ∼4 nm diameter that have been mesostructured through a self-assembling procedure with a block copolymer. These CeO_2 nanoparticles were embedded within ultrathin layers of highly structured SiO_2 binder. The resultant material presents surface areas above 300 $m^2\ g^{-1}$ and gives the most stable, while active and chemoselective, Pt-supported catalysts we are aware of for the hydrogenation of crotonaldehyde.

Experimental Section

Materials. The composite material was prepared from colloidal CeO_2 nanoparticle building blocks and the formation of mesostructured silica together with the simultaneous inclusion of CeO_2 nanoparticles. The assembly process was controlled by adjusting the interactions of a copolymer template with the CeO_2 nanoparticles and SiO_2. More specifically, a water, acid colloidal dispersion of CeO_2 nanoparticles (≈4 nm) was poured into an aqueous solution of poly(alkylene oxide) block copolymer ($EO_{20}PO_{70}EO_{20}$, Pluronic P123, BASF). Then TEOS was added at room temperature into the dispersion with stirring for 60 min. The resulting dispersion was aged at 318 K for 16 h and a precipitate was formed. The mixture was aged overnight at 353 K without stirring. The solid product (SiO_2–CeO_2, $C_{CeO_2} = 0.5$ M) was recovered, washed with water, and air-dried at 353 K. The copolymer template was removed by slowly increasing the calcination temperature from 293 to 773 K in 6 h, staying at this temperature for 6 h. The BET surface area of the resulting material was 376 $m^2\ g^{-1}$. A similar procedure but without introduction of the silica was used to prepare a mesostructured CeO_2 material, whose BET surface area after calcination was 166 $m^2\ g^{-1}$.

Pt/CeO_2-SiO_2 (1, 3, and 5 wt % Pt) and Pt/CeO_2 (1 wt % Pt) catalysts have been prepared by wet impregnation of the CeO_2-SiO_2 support and CeO_2 support with an aqueous solution of $[Pt(NH_3)_4](NO_3)_2$ (Aldrich), dried at 353 K, and calcined in air at 673 K for 4 h.

Characterization. SAXS data for the support material were collected and corrected for the scattering of the background.

Transmission electron microscopy (TEM) micrographs were obtained on a JEOL 1200X electron microscope operating at 120 keV. The samples for TEM were prepared directly by dispersing the powders onto carbon copper grids. For crystal analysis and indexation, the samples were examined by bright-field and dark-field transmission electron microscopy in a Field Emission JEOL 2200 high-resolution (HR) TEM operated at an accelerating voltage of 200 kV. Dark-field TEM consists of observing the image produced by the diffracted electrons instead of the transmitted ones. Dark-field imaging provides direct observation of the metallic nanoparticles (NP) within the oxide channels.

X-ray diffraction analysis (XRD) of the catalyst was obtained by use of a Phillips 1060 diffractometer provided with graphite monochromator employing nickel-filtered Cu Kα radiation ($\lambda = 0.1542$ nm). CeO_2 particle size was determined from the half-height width of the (111) fluorite phase diffraction peak ($2\Theta = 27°$) by use of the Scherrer equation.

Temperature-programmed reduction (TPR) measurements on calcined catalysts were carried out on a U-shape quartz reactor with a Micromeritics (Autochem 2910) apparatus. About 100 mg of catalyst was first treated in argon at room temperature for 30 min. The samples were subsequently contacted with a H_2/Ar mixture (H_2/Ar molar ratio of 0.10 and a total flow of 50 $cm^3\ min^{-1}$) and heated, at a rate of 10 $K\ min^{-1}$, up to a final temperature of 1100 K.

X-ray photoelectron spectra (XPS) were obtained in a VG Escalab 210 spectrometer, by use of nonmonochromated Al Kα ($h\nu = 1486.6$ eV) X-ray radiation. To avoid photoreduction of ceria, the energy of the X-ray beam was limited to 100 W. Kinetic energies of photoelectrons were measured with a hemispherical electron analyzer working at constant pass energy of 50 eV. The pressure in the analyzing chamber was maintained at 750×10^{-6} Torr. The binding energy scales were regulated by setting the C1s transition at 284.5 eV. Before XPS measurements, catalyst samples were reduced in situ at 473 and 773 K under a H_2 flow (80 $cm^3\ min^{-1}$).

Fourier transform infrared (FTIR) experiments were conducted with a quartz infrared cell fitted with KRS-5 windows and an external furnace. The IR chamber is glass-blown to a conventional vacuum system with rotatory and turbomolecular pumps. Wafers of catalyst samples (10 $mg\ cm^{-2}$) were reduced in situ under static conditions at 473 and 773 K for 1 h. After the reduction treatment, the samples were cooled in a vacuum and pulses of CO were introduced at 298 K with calibrated volumes (1.55 cm^3). IR spectra were recorded on a PC-controlled Bio-Rad FTS-40A FTIR spectrophotometer.

Catalytic Test. The catalytic tests for the chemoselective hydrogenation of crotonaldehyde were carried out in a fixed-bed stainless steel tubular reactor (12 mm i.d., 340 mm length) equipped with a coaxial thermocouple for temperature profile.

Before the catalytic runs, the catalysts (100 mg, 0.2−0.6 mm particle size mixed with 0.4 g of SiC) were reduced in situ under flowing H_2 (50 $cm^3\ min^{-1}$) at low (473 K) and high (773 K) temperature for 1 h, at a heating rate of 5 $K\ min^{-1}$. Crotonaldehyde hydrogenation was performed at 353 and 303 K. The reduced catalysts were contacted with a reaction mixture (H_2/CROALD ratio of 60) formed by passing the hydrogen flow through a thermostabilized saturator (278 K) containing the unsaturated aldehyde. The reaction products were analyzed by on-line gas chromatography with a Rtx-WAX 30m semicapillary column.

Results and Discussion

Catalysts Characterization: XRD, TPR, and TEM. The ordering of the calcined CeO_2 arrays, embedded in ultrathin SiO_2 layers are observed through SAXS. The SAXS pattern, given in Figure 1, shows a diffraction peak centered at 11.0 nm. The 2-D X-ray diffraction pattern of a selected area show a hexagonal structure (inset of Figure 1). The material consists of an hexagonal array of nanoparticles as observed through TEM images (Figure 2), consistent with the SAXS data. Distribution of the CeO_2 nanoparticles in the thin layer of mineral was determined through high-magnification TEM to consist of a homogeneous distribution of perfectly individualized CeO_2 nanoparticles. TEM imaging indicates a constant interparticle spacing in the range of a single nanoparticles.

Wide-angle X-ray diffraction studies on Pt/CeO_2-SiO_2-supported catalysts confirm the crystalline nature of the nanostructured SiO_2-CeO_2 material. High-angle X-ray Bragg peaks were observed at 27.3, 31.8, 46.0, and 54.8, which are characteristic of CeO_2 fluorite structure. By taking the (111) line broadening of the fluorite phase of ceria and using the Scherrer equation, an estimation of mean ceria particle size gives values of 3.3 nm, which is in accordance with the mean ceria nanoparticle sizes used during the preparation procedure. This particle size is smaller than that reported previously for precipitated CeO_2 (15.9 nm),[25] CeO_2 supported on SiO_2 (5.8

(24) Bernal, S.; Calvino, J. J.; Cauqui, M. A.; Gatica, J. M.; Larese, C.; Perez Omil, J. A.; Pintado, J. M. *Catal. Today* **1999**, *50*, 175.

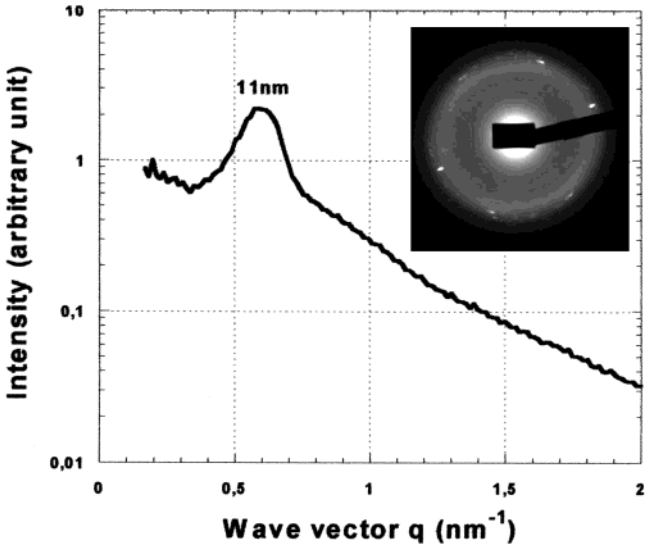

Figure 1. Small-angle X-ray diffraction pattern of CeO_2-SiO_2 materials. Inset: 2D SAXS of a selected area of calcined material, showing a hexagonal structure.

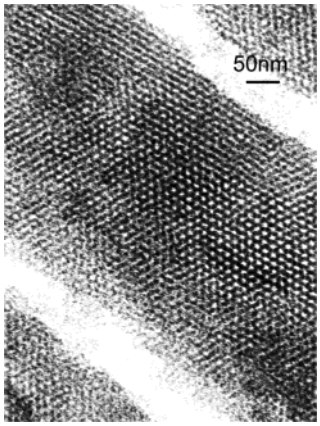

Figure 2. TEM micrographs of nanostructured CeO_2-SiO_2 materials showing hexagonal array domains.

nm),[26] and CeO_2 supported on carbon (4.2 nm).[27] Additionally, no lines corresponding to PtO_2, PtO, or Pt can be observed in the 2−70° 2Θ range for any of the Pt supported catalysts used here, this being an indication of the small metal particles present on the support after the calcination treatment at high temperature.

The redox behavior of the CeO_2-SiO_2 support in the presence or not of Pt has been studied by temperature-programmed reduction (TPR). Figure 3 shows the TPR profiles (hydrogen consumption against temperature) of (a) the mesoporous CeO_2-SiO_2 support and (b) the Pt/CeO_2-SiO_2 catalyst (1 wt % Pt). The mesoporous mixed oxide support exhibits two reduction peaks, the first one at low (736 K) temperature (0.98 mmol of H_2 g^{-1}) and the second one at high (950 K) temperature (0.88 mmol of H_2 g^{-1}). This behavior is in agreement with previously reported CeO_2 reductions,[25,28−31] with the low temperature reduction peak (at ca. 770 K) attributed to the reduction of the most easily reducible surface-capping oxygen of ceria and the second high-temperature peak (at ca. 1100 K) attributed to the bulk reduction of CeO_2. It is worth mentioning the high amount of hydrogen consumed in the low-temperature reduction peak with respect to the bulk process. This phenomenon can be related with the high proportion of surface CeO_2 species in the small nanoparticles present in the support. For the mesostructured CeO_2-SiO_2 support, the ceria surface reduction temperature appears close to that reported in the literature (736−770 K), although for the bulk reduction this value is downward shifted by 150 K. Traditionally, it has been assumed that this high-temperature reduction process was controlled by the slow bulk diffusion of the oxygen vacancies created at the surface of the oxide.[32] However, more recently Trovarelli and co-workers suggested that the surface reduction process and the difference of both thermodynamic and kinetic properties existing in the ceria microcrystals as a function of their size are the critical factors in determining the TPR trace of ceria.[30] With this in mind, the downward shift observed for the nanostructured CeO_2-SiO_2 support would be associated with the lower reduction enthalpy of high surface area nanocrystalline ceria in comparing with the bulk material, as obtained by the measurement of defect thermodynamics.[33,34]

The incorporation of Pt into the CeO_2-SiO_2 support completely modifies the TPR profile. Now, the surface ceria

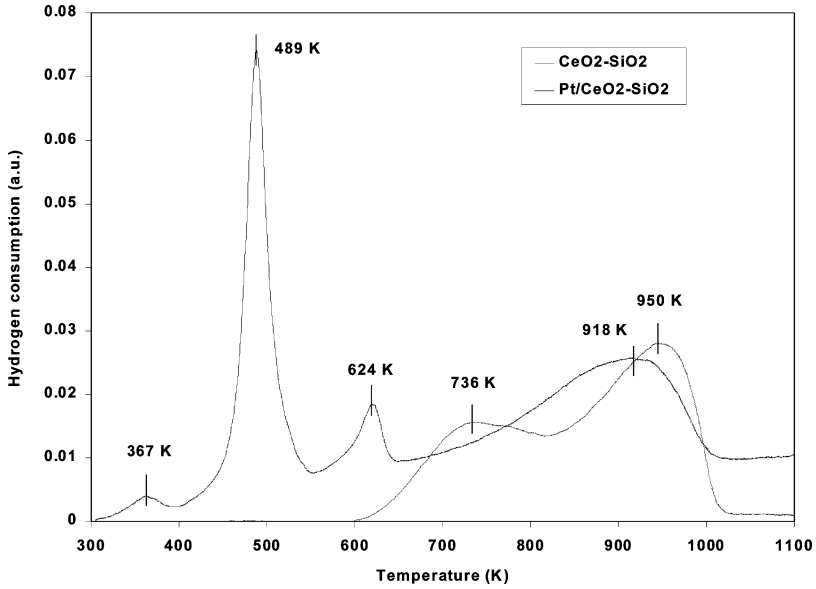

Figure 3. Temperature-programmed reduction (TPR) profiles for mesoporous CeO_2-SiO_2 (grey line) and Pt/CeO_2-SiO_2 (1 wt % Pt) catalyst (dark line).

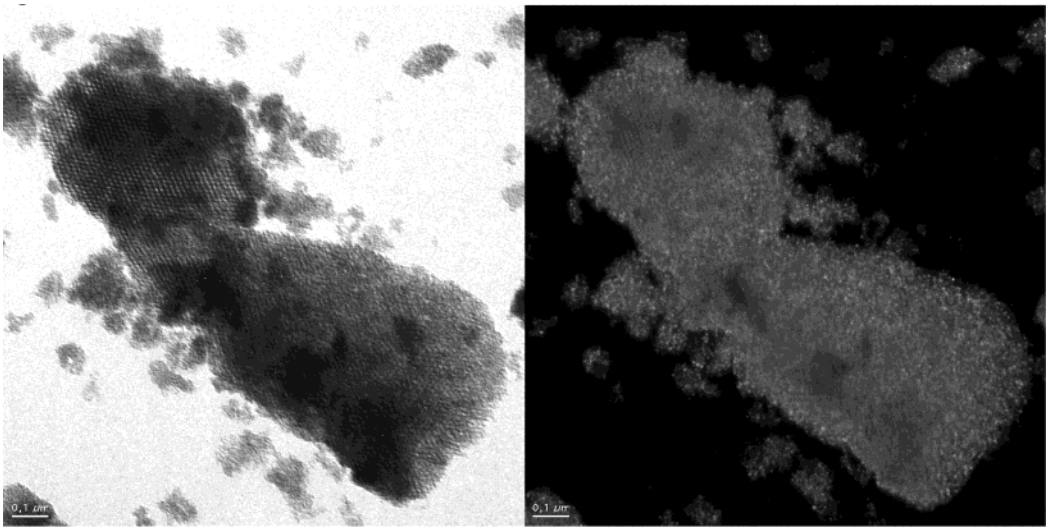

Figure 4. Bright-field (left) and dark-field (right) TEM images of 3 wt % Pt/CeO_2-SiO_2. The brighter spots on the right picture correspond to Pt crystals with the 111 direction perpendicular to the sample plane. The less bright crystals correspond to CeO_2 crystals with the 200 direction perpendicular to the sample plane.

reduction peak at 736 K is completely lacking, giving rise to three new low-temperature reduction peaks centered at 367, 489, and 624 K, together with the bulk ceria reduction centered at 918 K. The first hydrogen consumption at low temperature (367 K) corresponds to the reduction of oxidized Pt to Pt^0. In accordance with previous Pt/CeO_2 TPR studies,[25−27,29] this reduction process must be associated with noble metal particles that are not submitted to a strong metal−support interaction, i.e., Pt particles that are present over the SiO_2. The small hydrogen consumption associated with this reduction peak would be either an indication of a preference of Pt particles by CeO_2 nanoparticles or a consequence of high Pt reduction during the calcination treatment. The second reduction peak at 489 K corresponds to the surface reduction of CeO_2 in close contact with the noble metal particles, as well as to the breakdown of $Pt-O-CeO_2$ entities formed upon the calcination treatment. This shift in the surface ceria reduction with Pt addition can be related with the presence of hydrogen spillover processes from the noble metal surface.[25,29−31] The other mild temperature reduction peak at 624 K can be related to the surface reduction of ceria not in close contact with Pt. Finally, the high-temperature reduction peak at 918 K is associated with the bulk reduction of CeO_2, a reduction peak that has been slightly shifted to lower temperatures after Pt addition (from 950 to 918 K). This result differs from the literature, where the bulk CeO_2 reduction is shown to be unaffected by the noble metal presence.[25,29,35−36] However, the smaller CeO_2 particle sizes present in this case, together with the different thermodynamic and kinetic properties of the ceria microcrystals after Pt addition, can be responsible for the behavior observed.

In conclusion, the TPR profiles show the characteristic peaks of CeO_2 corresponding to the surface and bulk reduction, both processes being shifted to lower temperatures by Pt addition.

The morphological analysis of the different Pt catalysts after the calcination treatment has been carried out by transmission electron microscopy (TEM). Figure 4 shows the TEM analysis of the Pt/CeO_2-SiO_2 (3 wt % Pt) catalyst. As can be seen, the mesoporous structure constituted of wormlike and ordered channels organized into hexagonal arrays shown before for the CeO_2-SiO_2 was preserved after Pt incorporation and the subsequent thermal treatment. The pore size is fairly monodispersed and is between 6 and 9 nm in diameter, a value that is in agreement with the SAXS analysis and the wall thickness values. The observed platinum nanoparticles are all located onto the support, are not agglomerated, and have a mean diameter of 2−3 nm, suggesting that the Pt has been successfully encapsulated inside the pores. Pt particle size distribution histograms for Pt/CeO_2-SiO_2 catalysts with 1 and 3 wt % Pt are plotted in Figure 5. When the two samples are compared, the catalyst with the higher metal loading shows a narrower size distribution with the mean Pt particle size centered at 3 nm.

A series of energy-dispersive X-ray elemental mapping images of the calcined samples showed the following: the Pt concentration is larger (10%) in the most crystalline grains, probably due to a larger porosity, and the Pt particles show a preference for the CeO_2 nanoparticles (≈70% of the Pt would be on ceria grains while the rest would be on silica). This observation would be in accordance with the presence of specific metal−ceria interactions (SMSI) that further stabilize the platinum particles through $Pt-O-CeO_2$ entities formation.[37,38]

(25) Sepúlveda-Escribano, A.; Coloma, F.; Rodriguez-Reinoso, F. *J. Catal.* **1998**, *178*, 649.
(26) Silvestre-Albero, J.; Rodriguez-Reinoso, F.; Sepúlveda-Escribano, A. *J. Catal.* **2002**, *210*, 127.
(27) Sepúlveda-Escribano, A.; Silvestre-Albero, J.; Coloma, F.; Rodriguez-Reinoso, F. *Stud. Surf. Sci. Catal.* **2000**, *130*, 1013.
(28) Yao, H. C.; Yao, Y. F. Y. *J. Catal.* **1984**, *86*, 254.
(29) de Leitenburg, C.; Trovarelli, A.; Kaspar, J. *J. Catal.* **1997**, *166*, 98.
(30) Giordano, F.; Trovarelli, A.; de Leitenburg, C.; Giona, M. *J. Catal.* **2000**, *193*, 273.
(31) Trovarelli, A. *Catalysis by ceria and related materials*; Catalytic Science Series; Hutchings, G. J., Ed.; Imperial College Press: London, 2002; Vol. 2, pp 100−102.
(32) El Fallah, J.; Boujana, S.; Dexpert, H.; Kiennemann, A.; Majerus, J.; Touret, O.; Villain, F.; Le Normand, F. *J. Phys. Chem.* **1994**, *98*, 5522.
(33) Hwang, J. H.; Mason, T. O. *Z. Phys. Chem.* **1998**, *207*, 21.
(34) Chiang, Y. M.; Lavick, E. B.; Kosacki, I.; Tuller, H. L.; Ying, J. Y. *J. Electroceram.* **1997**, *1*, 7.
(35) Holgado, J. P.; Munuera, G. *Stud. Surf. Sci. Catal.* **1995**, *96*, 109.
(36) Bernal, S.; Botana, F. J.; Garcia, R.; Ramirez, F.; Rodriguez-Izquierdo, J. M. *Mater. Chem. Phys.* **1987**, *18*, 119.
(37) Brogan, M. S.; Dines, T. J.; Cairns, J. A. *J. Chem. Soc., Faraday Trans.* **1994**, *90*, 1461.
(38) Murrel, L. L.; Tauster, S. J.; Anderson, T. R. *Stud. Surf. Sci. Catal.* **1991**, *71*, 275.

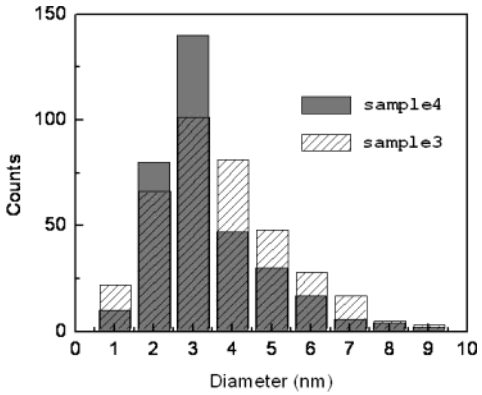

Figure 5. Size distribution histogram of the Pt particles formed and dispersed in the mesoporous silica−Ceria matrix. Sample 3, Pt/CeO_2−SiO_2 (1 wt % Pt); sample 4, Pt/CeO_2−SiO_2 (3 wt % Pt).

Besides, no difference in the noble metal morphology was observed depending on the support, either ceria or silica.

The crystal lattice of the metallic Pt nanoparticle is observed in the high-resolution TEM images shown in Figure 6. To determine the lattice spacing, the inverse of the radius of the dots or rings that appear in the FFT of the image was taken. By doing this, the following preferential orientations were observed: 200 Pt, 110 CeO_2, and 011 CeO_2 of the face-centered cubic (fcc) Pt and rhombohedric CeO_2.

Summarizing, while the SiO_2 nanodomains are amorphous, the CeO_2 particles are highly crystalline with a grain size distribution remarkably narrow with an average size about 3−4 nm. As one may expect, such small crystals appear faceted, displaying flat terraces and sharp edges. While the surface-to-volume ratio decreases for round particles, faceted crystals occur often for noble metal 2−3 nm particles, or atomic clusters, which serves to expose the same atoms density (reactivity) in all the surfaces. Pt crystals appear blended with the CeO_2 ones, with similar sizes, size distribution, and shapes, indicating that the original CeO_2 crystal size limited the growth of larger Pt crystals. This support-induced growth leads to small and narrow size distributions, significantly smaller and narrower than those obtained by Pt impregnation on conventional CeO_2.

From XRD and TEM results we can conclude that mesostructured CeO_2−SiO_2 samples mainly within an hexagonal array have been obtained. The structure is preserved upon Pt

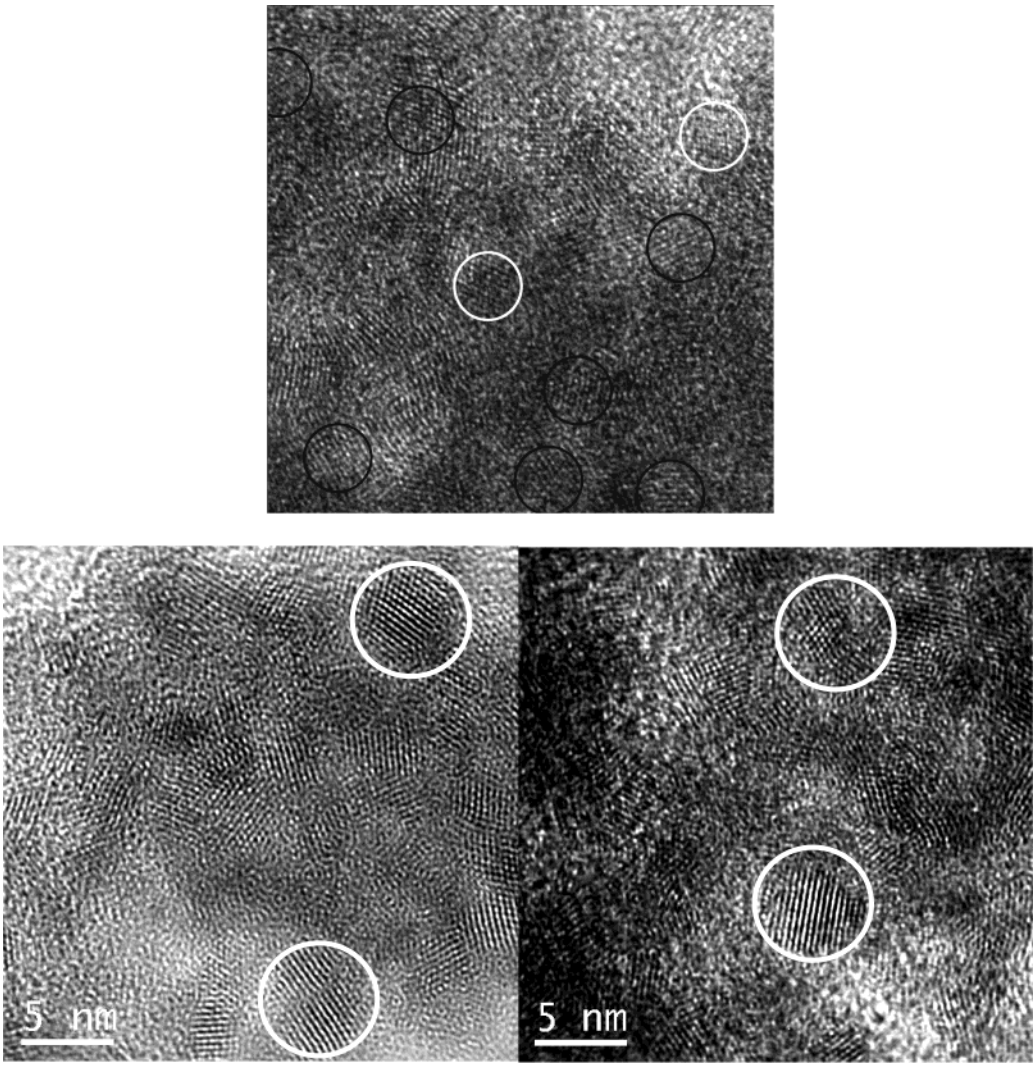

Figure 6. (a, upper panel) High-resolution TEM of the SiO_2−CeO_2−Pt composite. Black circles indicate crystals showing the 111 and 200 CeO_2 fringes, and the white ones indicate crystals showing the 111 and 200 Pt planes. (b, lower panels) High-resolution TEM of the Pt particles. On the left image, the black circle indicates a crystal showing the 200 CeO_2 fringes and the white one indicates a crystal showing the 111 Pt plane. On the right image, a cubic (bottom) and a faceted crystal (top) are circled.

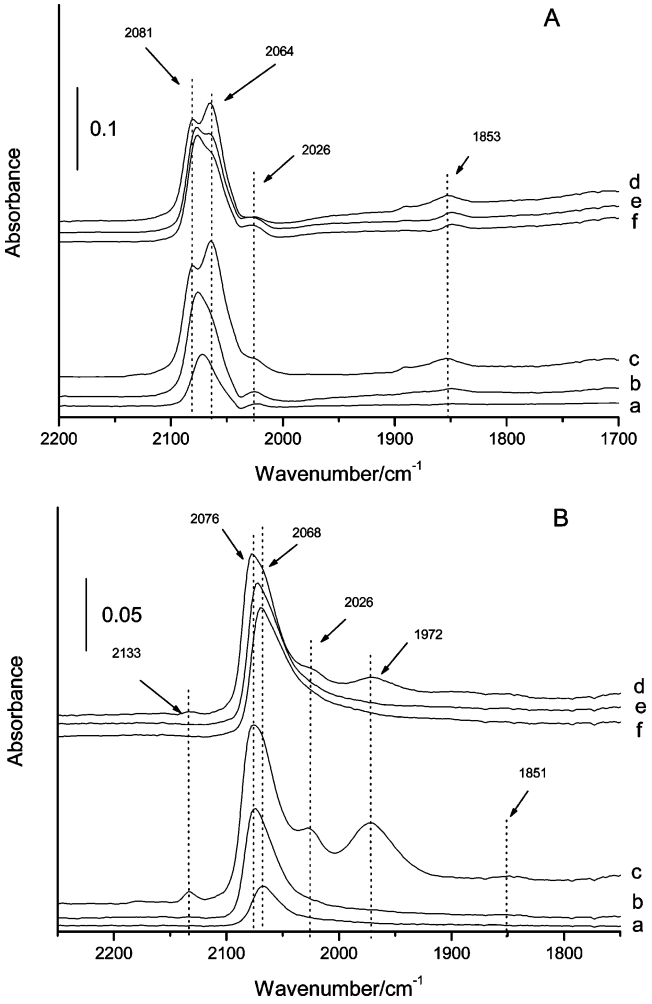

Figure 7. FTIR spectra of Pt/CeO_2-SiO_2 (1 wt % Pt) catalyst reduced at (A) 473 K and (B) 773 K and exposed to (a) 0.3, (b) 15, and (c) 300 Torr (crucible pressure) CO and then outgassed for (d) 0.5, (e) 5, and (f) 30 min.

deposition and catalyst activation. Pt incorporation shows a preference for CeO_2 particles and its interaction clearly affects the reducibility of the support and the metal. There is a very narrow distribution of Pt crystal size with a maximum at 3 nm. Moreover, practically all the particles correspond to faceted crystals. Then, from a catalytic point of view and before any adsorption or reactivity studies are performed, the Pt/CeO_2-SiO_2 catalyst already appears as quite a unique and interesting material.

CO Adsorption Studies. FTIR spectra of reduced samples prior to CO adsorption shows one band at 3747 cm^{-1}, corresponding to the OH-stretching vibration of Si−OH groups, which is not modified after CO adsorption (spectra not shown). No bands in the 2300−1700 cm^{-1} region or in the carbonate region are observed. Figure 7 shows the IR spectra of CO adsorbed at 298 K on Pt/CeO_2-SiO_2 (1 wt % Pt) catalysts after a low-temperature (473 K) and a high-temperature (773 K) reduction treatment. Adsorption of 0.3 Torr CO on the Pt/CeO_2-SiO_2 catalyst reduced at 473 K (Figure 7A) leads to appearance of a broad asymmetric band with a maximum at 2072 cm^{-1}. When CO pressure is increased, the main band is slightly shifted toward higher frequencies (2081 cm^{-1}), while a shoulder at 2064 cm^{-1} becomes evident. This increases in intensity with increasing CO surface coverage. The Pt−CO IR band at 2081 cm^{-1} is indicative of the presence of metal atoms in less dense close packing arrangements such as 100 faces, while the CO low-frequency band at 2064 cm^{-1} is related to the presence of Pt atoms in defect sites (steps and corners).[39,40] These results are in agreement with the observations made previously by TEM. Additionally, a small band at 2026 cm^{-1} appears also at low CO coverages and remains practically unchanged after an evacuation treatment during 30 min. This low-frequency IR band can be attributed to CO adsorption on noble metal atoms interacting with an electron-donor center from the support.[41,42] Indeed, we have detected by XPS the formation of Ce^{3+} ions and oxygen vacancies during the reduction of ceria at low temperature, and these Ce^{3+} ions may act as electron-donor centers to the platinum. Such an electron transfer will reinforce the back-donation from Pt to CO, giving rise to the low-frequency value described (2026 cm^{-1}) and to the higher stability of the band toward the evacuation treatment. The formation of the 2026 cm^{-1} band can be also due to a secondary interaction of the Pt−CO species with defect sites of the support, which should cause the lateral tilt of the CO group.[40] On the other hand, when the CO pressure is increased, a broad contribution at 1853 cm^{-1} also appears that is associated with CO adsorbed in a 2-fold bridging mode on Pt sites.[39,40,43] CO evacuation experiments at 298 K show a high stability of the 2026 cm^{-1} band and the band at 2081 cm^{-1}, which is red-shifted by decreasing CO coverage, while the bands at 2064 and 1853 cm^{-1} are less stable (see Figure 7A).

An increase in the reduction temperature from 473 to 773 K produces important changes in the CO spectrum (Figure 7B). At low CO coverages the spectrum shows a broad peak at 2067 cm^{-1} together with a tail at lower frequencies. After CO pressure is increased, the main band is blue-shifted to 2076 cm^{-1} and a shoulder at 2068 cm^{-1} became evident. According to the literature, the low-frequency IR bands at 2076 and 2068 cm^{-1} correspond to CO adsorbed on low-coordinated Pt sites, i.e., Pt in defect sites, which are indicative of small particle sizes of the Pt crystallites.[44] Increasing CO coverage also produces the appearance of additional bands at 2133, 2026, and 1972 cm^{-1}, while the band at 1853 cm^{-1} is practically absent. The band at 2133 cm^{-1} can be assigned to CO−Ce^{3+} entities.[42,45,46] It should be pointed out that the intensity of the band at 2026 cm^{-1}, attributed to CO species adsorbed on Pt particles influenced by the CeO_2 support (either electronically or morphologically), compared to the intensity of the bands due to CO species adsorbed linearly on Pt sites is higher for the samples reduced at 773 K than for the sample reduced at 473 K (intensity ratio of distorted CO/linear CO of 0.42 and 0.15, respectively). This can be related to a higher reduction of the CeO_2 support at increasing reduction temperatures (i.e., higher amount of Ce^{3+} or defect sites) and to the small particle size of the Pt crystallites. The band at 1972 cm^{-1} disappears easily under vacuum

(39) Binet, C.; Badri, A.; Lavalley, J. C. *J. Phys. Chem.* **1994**, *98*, 6392.
(40) Bensalem, A.; Muller, J. C.; Tessier, D.; Bozon-Verduraz, F. *J. Chem. Soc. Faraday Trans.* **1996**, *92*, 3233.
(41) Silvestre-Albero, J.; Sepúlveda-Escribano, A.; Rodriguez-Reinoso, F.; Anderson, J. A. *Phys. Chem. Chem. Phys.* **2003**, *5*, 208.
(42) Tanaka, T.; White, J. M. *J. Catal.* **1983**, *79*, 81.
(43) Coloma, F.; Coronado, J. M.; Rochester, C. H.; Anderson, J. A. *Catal. Lett.* **1998**, *51*, 155.
(44) Bozon-Verduraz, F.; Bensalem, A. *J. Chem. Soc., Faraday Trans.* **1994**, *90*, 653.
(45) Zaki, M. I.; Viekhaber, B.; Knözinger, H. *J. Phys. Chem.* **1986**, *90*, 3176.
(46) Yu. Stakheev, A.; Shpiro, E. S.; Jaeger, N. I.; Schulz-Ekloff, G. *Catal. Lett.* **1995**, *34*, 293.

conditions and has been assigned to Pt-dicarbonyl species.[47] The presence of the last band in the Pt/CeO_2-SiO_2 sample reduced at 773 K, which is not present in the sample reduced at 473 K and in previous FTIR studies of adsorbed CO over Pt/CeO_2,[44] can be related to the high amount of low-coordinated, highly unsaturated Pt sites. This assignation will be in agreement with the fact that the band at 1853 cm^{-1}, assigned to bridge CO species, was not observed in our case.[48]

Finally, the FTIR spectra of adsorbed CO over a Pt/CeO_2 catalyst submitted to a reduction treatment at 773 K has been studied (spectra not shown). Prior to CO adsorption, IR bands at 3747 cm^{-1}, referred to OH hydroxyl groups, and IR bands at 1526, 1470, 1397, and 1368 cm^{-1} due to carbonate compounds are observed. No bands in the 2300−1700 cm^{-1} region are present. After CO adsorption, intense IR bands attributed to linear adsorbed CO and Pt-dicarbonyl species are observed (spectra not shown), followed with the appearance of new bands in the 1600−1000 cm^{-1} region, due to carbonate formation. Carbonate formation due to decomposition of adsorbed CO to CO_2 and carbon has been reported in the literature at high adsorption temperatures.[49] On the other hand, CO_2 formation from adsorbed CO with the participation of lattice oxygen from the support in the interface between Pt and CeO_2 can also be considered. In this case, a reaction mechanism in which CO dosed from the gas phase adsorbs on the Pt terrace, equilibrates among more stable corner or step sites, and migrates to the interface where it picks up a lattice oxygen and forms CO_2, has been proposed.[50]

Worth mentioning is the absence of the IR band at 2026 cm^{-1} (observed on Pt/CeO_2-SiO_2 samples), which has been previously attributed to linear Pt−CO species partially distorted by defect sites at the metal−support interface. Probably, the blockage of defect sites at the $Pt-CeO_2$ interface by CO_2 formation can be responsible for the observed behavior.

According to our results, the presence or absence of the low-frequency IR band at 2026 cm^{-1} is related to the presence or not of special Pt sites at the contact perimeter of the metal particle with the support. These sites show a promoting effect in the activation of the CO bond and therefore can act as possible active sites in the chemoselective hydrogenation of crotonaldehyde.

XPS Characterization. XPS spectra of the Pt 4f, O 1s, Si 2s, and Ce 3d core levels of calcined and in situ reduced (at 473 and 773 K) samples have been collected and shown in Figure 8 for the Pt/CeO_2-SiO_2 (1 wt % Pt) sample. It can be seen there that the Pt 4f core-level XPS spectrum is shifted to lower binding energies by reduction of the sample and a broadening of the spectrum is clearly observed after low-temperature reduction (473 K). Deconvolution of the Pt $4f_{7/2}$ peak has revealed only one component in the calcined sample at binding energy 72.8 eV (fwhm 2.3 eV), which has been attributed to Pt^{2+} species in PtO.[51] In the reduced sample at 473 K the broadening of the Pt 4f core-level spectrum is due to the presence of more than one component, since no broadening is observed in the XPS spectra of the other elements. In this sense, the presence of two components at BE 72.2 and 71.0 eV (fwhm 2.4 and 2.5 eV, respectively) can be deduced. Finally the Pt $4f_{7/2}$ core-level spectrum of the reduced sample at 773 K shows the presence of only one component at BE 71.2 eV (fwhm of 2.3 eV). While binding energies about 70.5−70.7 eV are characteristic of metallic platinum,[52−54] the shift of the Pt 4f binding energy to higher values (71.2 eV) has been attributed to final state effects due to reduced screening of the photo hole after electron emission in small particles.[55] In fact, we have observed the presence of small particles by TEM and IR spectra of adsorbed CO. The presence of both Pt^{2+} and Pt^0 species (Pt^{2+}/Pt^0 atomic ratio = 0.7) in the 473 K reduced sample does not agree with the TPR results, which shows a high reducibility of the Pt but can be explained by diffusional problems in the reduction process in the XPS microreactor.

The XPS spectra of the Ce 3d core level have been fitted into several components in accordance with Burroughs and coworkers.[56] The Ce^{4+}/Ce^{3+} atomic ratio has been obtained from the area of the peaks obtained by the deconvolution procedure. In this way a $Ce^{3+}/(Ce^{4+} + Ce^{3+})$ ratio of 0.1 has been obtained on the calcined sample, while the amount of Ce^{3+} species increases appreciably after high reduction temperature [$Ce^{3+}/(Ce^{4+} + Ce^{3+})$ atomic ratio of 0.54].

The O1s XPS spectrum shows the presence of two oxygen components at BE 532.9 and 530.0 eV, corresponding to SiO_2 and CeO_2, respectively. These indicate that oxygen arising from carbonate impurities also appears around 532 eV, which could lead to some errors if quantitative measurements are required. However, it can be said on a qualitative bases that the oxygen component at BE 530.3 eV decreases by increasing reduction temperature, something that could be assigned to oxygen loss by reduction of the CeO_2 support.

Thus, from the XPS spectra of the Pt/CeO_2-SiO_2 sample the presence of small Pt^0 particles and a high reduction degree ($Ce^{4+} \rightarrow Ce^{3+}$) of the CeO_2 support is inferred. On the other hand, a substantial decrease in the peak area of the Ce 3d/Si 2s core levels in the Pt/CeO_2-SiO_2 sample compared to the pure CeO_2-SiO_2 support has been seen. This decrease in the peak areas can be attributed to a preferential localization of the Pt particles on the ceria nanoparticles, in agreement with the results obtained by HREM.

Nanostructured Pt/CeO_2 catalyst has also been studied by XPS, and large differences with respect to the Pt/CeO_2-SiO_2 sample have been observed. The Pt 4f XPS spectrum shows the presence of Pt^{2+} species on the calcined sample, while Pt^0 is observed on the sample reduced at 773 K. However, a lower BE of the Pt $4f_{7/2}$ core level is observed (70.9 eV), which is characteristic of metallic Pt^0 particles. In this sense, higher particle sizes can be inferred in the Pt/CeO_2 sample in contrast to the small particle size observed in the Pt/CeO_2-SiO_2 sample. On the other hand, the Ce 3d XPS spectra shows a lower reduction degree of the Ce ions after in situ reduction of the Pt/CeO_2 sample in H_2 at 773 K [$Ce^{3+}/(Ce^{4+} + Ce^{3+}) = 0.27$].

(47) Jin, T.; Zhou, Y.; Mains, G. J.; White, J. M. *J. Phys. Chem.* **1987**, *91*, 5931.
(48) Dulaurent, O.; Chandes, K.; Bouly, C.; Bianchi, D. *J. Catal.* **1999**, *188*, 237.
(49) Bourane, A.; Dulaurent, O.; Bianchi, D. *J. Catal.* **2003**, *195*, 6.
(50) Jin, T. *J. Phys. Chem.* **1987**, *91*, 5931.
(51) Drawdy, J. E.; Hoflund, G. B.; Gardner, S. D.; Yngvadottir, E.; Schryer, D. R. *Surf. Interface Anal.* **1990**, *16*, 369.
(52) Huidobro, A.; Sepulveda-Escribano, A.; Rodriguez-Reinoso, F. *J. Catal.* **2002**, *212*, 94.
(53) Duekers, K.; Bonzel, H. P. *Surf. Sci.* **1989**, *213*, 25.
(54) Mullins, D. R.; Zhang, K. Z. *Surf. Sci.* **2002**, *513*, 163.
(55) Henry, C. R. *Surf. Sci. Rep.* **1998**, *31*, 231.
(56) Burroughs, P.; Hammett, A.; Orchard, A. F.; Thomton, G. J. *J. Chem. Soc., Dalton Trans.* **1976**, *17*, 1686.

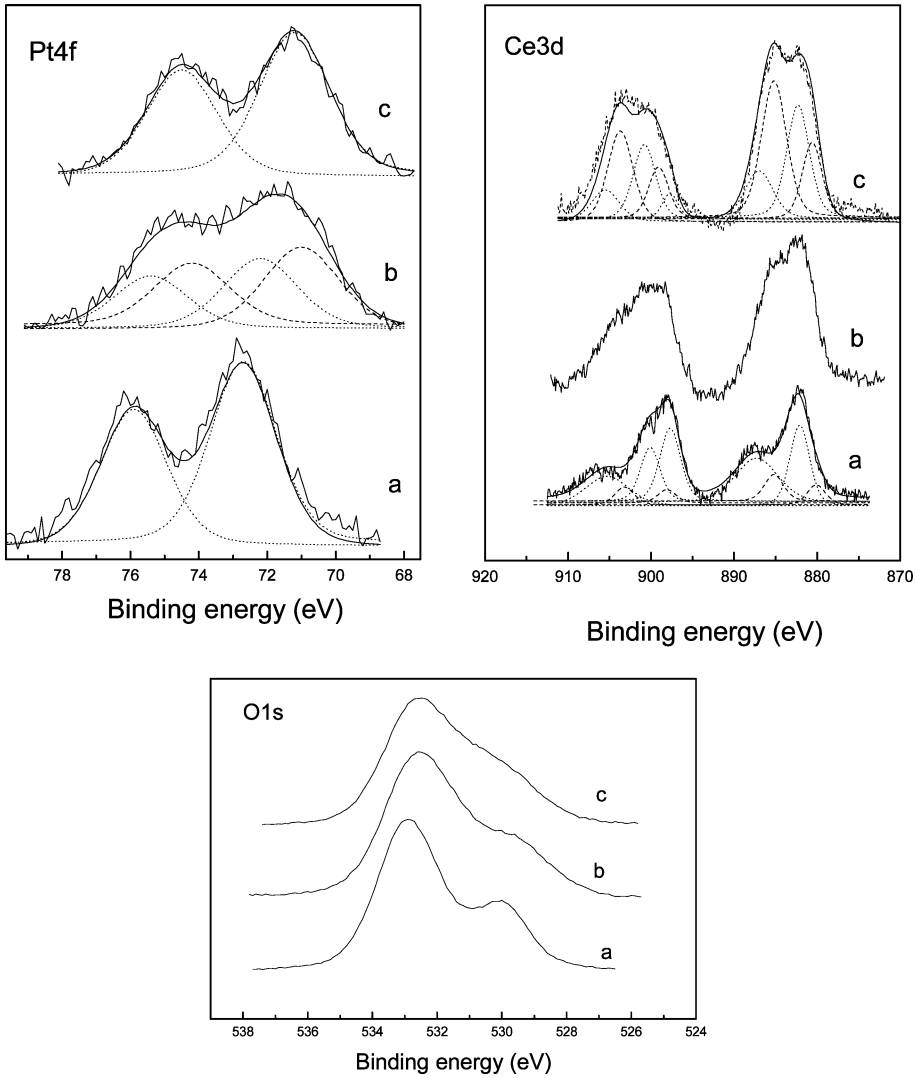

Figure 8. Pt 4f, Ce 3d, and O 1s core-level photoelectron spectra of the 1 wt % Pt/CeO_2-SiO_2 catalyst (a) calcined, (b) reduced at 473 K, and (c) reduced at 773 K. Broken lines show deconvoluted peaks.

At this point, we can claim the presence of small Pt metal particles mainly located on the CeO_2 nanoparticles of the Pt/CeO_2-SiO_2 catalyst, with a high proportion of $Pt-CeO_{2-x}$ interfacial sites, which should favor the activation of the C=O bond leading to a high selectivity toward unsaturated alcohol formation.

Catalytic Behavior. The effect of the reduction temperature and noble metal loading on these Pt/CeO_2-SiO_2 and Pt/CeO_2 catalysts have been studied in the vapor-phase chemoselective hydrogenation of crotonaldehyde at both 353 and 303 K. Figure 9 shows the evolution of the overall activity (micromoles of CROALD transformed per gram of platinum per second) at 353 K as a function of time on stream for the Pt/CeO_2-SiO_2 (1 wt % Pt) catalyst after low- and high-temperature reduction treatment. The catalytic results were obtained once the carbon balance was achieved, i.e., once the amount of crotonaldehyde leaving the reactor matched that fed minus the amount transformed into reaction products. As can be seen there, while the overall activity after a low-temperature reduction treatment is mainly constant at 27 μmol of CROALD (g of Pt)$^{-1}$ s^{-1}, an increase in the reduction temperature to 773 K produces an increase in the initial activity together with a strong deactivation during the first reaction minutes down to a quasi steady state around 22 μmol of CROALD (g of Pt)$^{-1}$ s^{-1}. Polymerization and decarbonylation processes during the first minutes of reaction appear to be responsible for the high deactivation observed. The increase of the initial catalytic activity after a high-temperature reduction treatment is very similar to that reported previously for a 1% Pt/CeO_2 catalyst in the title reaction.[25] Abid and Touroude[57] observed a decrease in the overall catalytic activity for the vapor-phase hydrogenation of crotonaldehyde over 5% Pt/CeO_2 catalysts, prepared from chlorinated and chlorine-free precursors, when the reduction temperature was increased from 473 to 873 K, although the reported results were obtained at steady-state conditions. It is also worth mentioning that this catalytic behavior is completely different from that obtained over $Pt/CeO_2/SiO_2$ [26] and Pt/SiO_2 [25] catalysts, where an increase in the reduction temperature gives rise to a decrease in the overall catalytic activity. Despite the Pt sintering process with increasing reduction temperature, which would lead to a decrease in the catalytic activity, the presence of CeO_2 modifies the catalytic behavior of Pt catalysts, probably by electronic effects induced after the high-temperature reduction treatment.

(57) Abid, M.; Touroude, R. *Catal. Lett.* **2000**, *69*, 139.

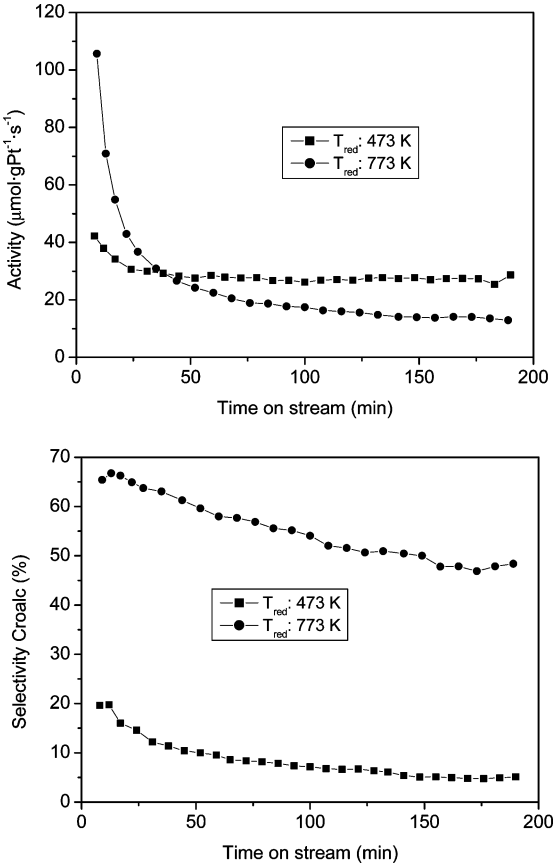

Figure 9. Evolution of the overall catalytic activity (in micromoles per gram of platinum per second) and the selectivity toward crotyl alcohol formation at 353 K versus time on stream for a Pt/CeO_2-SiO_2 catalyst (1 wt % Pt) after low- and high-temperature reduction treatment.

The products formed under the reaction conditions used in our study are butyraldehyde, which comes from C=C bond hydrogenation; crotyl alcohol, produced by C=O hydrogenation; butanol, which is the completely saturated product produced in secondary hydrogenation reactions; and finally light hydrocarbons such as butane and propane, produced by further hydrogenation and decarbonylation reactions. Figure 9 shows the evolution of the selectivity toward crotyl alcohol formation for the Pt/CeO_2-SiO_2 (1 wt % Pt) catalyst after reduction treatment at low and high temperature. These results reveal that an increase of the reduction temperature from 473 to 773 K for the Pt/CeO_2-SiO_2 catalyst produces a strong increase of the crotyl alcohol selectivity from 10% up to 60% at 353 K. On the other hand, the FTIR−CO adsorption and XPS results presented above clearly show that by increasing the reduction temperature, the number of $Pt-CeO_{2-x}$ interfacial sites increases, these sites being responsible for activating the carbonyl groups. This activation will increase the rate of hydrogenation of the C=O groups, increasing the selectivity toward the formation of the desired unsaturated alcohol.

The crotyl alcohol selectivity profile with time on stream (Figure 9) over 1% Pt/CeO_2-SiO_2 catalyst exhibits some deactivation, which could be related to the presence of secondary reactions that are favored at high reaction temperatures. Therefore, the reaction has been carried out at lower temperatures (303 K). Decreasing the reaction temperature from 353 to 303 K for the Pt/CeO_2-SiO_2 catalyst reduced at high temperature (773 K) produces a slight decrease of the catalytic activity down

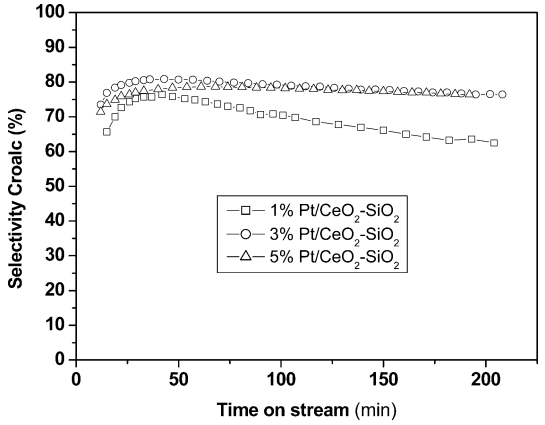

Figure 10. Evolution of the selectivity to crotyl alcohol as a function of time on stream for the different Pt/CeO_2-SiO_2 catalysts in the selective hydrogenation of crotonaldehyde at 303 K. Previous to catalytic reaction catalysts have been reduced at 773 K.

Table 1. Catalytic Activities and Selectivities for Different Pt/CeO_2-SiO_2 and Pt/CeO_2 Catalysts in the Chemoselective Hydrogenation of Crotonaldehyde at 303 K. T_{Red}: 773 K

catalyst	wt % Pt	activity [μmol (g of Pt)$^{-1}$ s^{-1}]	selectivity Croalc (%)	conversion (%)
Pt/CeO_2-SiO_2	1	16.4	75	2.7
Pt/CeO_2-SiO_2	3	17.0	81	9.6
Pt/CeO_2-SiO_2	5	21.0	80	18.9
Pt/CeO_2	1	2.6	38	0.5

to 16.4 μmol of CROALD (g of Pt)$^{-1}$ s^{-1}, while the selectivity to crotyl alcohol is further improved up to a final value close to 75% after 60 min on stream. Indeed, this improvement in the selectivity at low reaction temperatures is associated with the suppression of secondary processes, which are favored at higher temperatures and which acts against crotyl alcohol selectivity.

An increase in the Pt content from 1 to 5 wt % produces an improvement in the catalytic activity and selectivity (Table 1). It has to be remarked that with the higher Pt-containing catalyst the selectivity remains unchanged with time on stream, not showing any sign of deactivation, at least for the time period studied here (Figure 10). Moreover, when conversion was modified from 2% to 20% by changing contact time, selectivity remained constant at ~80%.

When we considered the TEM results, which showed that 70% of the Pt was supported on CeO_2 while 30% was located on SiO_2, we though the loss of chemoselectivity to be due to the Pt supported on SiO_2. Thus, it appeared logical to prepare a catalyst in where the Pt was supported on a pure mesostructured CeO_2 support with a high surface area (166 m^2 g^{-1}).

After reduction at 773 K, the catalytic results obtained with this catalyst (Pt/CeO_2) show (Table 1) a lower activity and selectivity than those obtained with the Pt/CeO_2-SiO_2 catalyst. This low selectivity value obtained when nanostructured CeO_2 was used as a support can be related to the absence of the IR band at 2026 cm^{-1}, which has been attributed to Pt sites at the metal−support interface. This can be related to the higher particle size as inferred from the XPS results and/or to the high proportion of carbonate species in the $Pt-CeO_2$ interface as deduced from IR spectroscopy.

We have compared in Table 2 the activity and selectivity of the Pt/CeO_2-SiO_2 catalyst reported here with the best Pt

Table 2. Comparison of the Catalytic Activities and Selectivities for Different Pt/MO_x Catalyst in the Selective Hydrogenation of Crotonaldehyde

catalyst	reduction temp (K)	reaction temp (K)	activity [μmol (g of Pt)$^{-1}$ s^{-1}]	selectivity (%)	ref
Pt/SnO_2	443	353	13	77	50
	443	303	4.2[a]		
Pt/CeO_2	973	353	2.1	83	46
	973	303	0.7[a]		
Pt/ZnO	673	353	1.6	81	49
	673	303	0.5[a]		
$Sn-Pt/SiO_2$		333	0.9	90	40
		303	0.16		
Pt/CeO_2-SiO_2	773	303	21.0	80	

[a] Catalytic activity values obtained considering a typical apparent activation energy for the title reaction of 20 kJ mol^{-1}.[58]

catalysts previously reported for the title reaction. The values given clearly show that Pt on the nanostructured CeO_2-SiO_2 support is highly selective and close to 1 order of magnitude more active than previously reported catalysts. It has to be remarked that the apparent activation energy for the hydrogenation of crotonaldehyde obtained with our catalyst is 12 kJ mol^{-1}, which is almost half of the 20 kJ mol^{-1} obtained on other supports.[58] This will indicate that by supporting the Pt on the nanostructured crystalline CeO_2 described here, we are changing the nature of the active sites by interaction of the nanocrystals of Pt with the nanocrystals of CeO_2. It may very well occur that the surface atoms of the very small crystals of CeO_2 show electronic properties different from those of the bulk. This, together with the very strong metal−support interaction showed by FTIR−CO adsorption and with XPS that predicts the formation of $Pt-CeO_{2-x}$ species as potential active sites, will explain the very high activity shown by the mesostructured Pt/CeO_2-SiO_2.

Conclusions

High surface area, thermally stable mesostructured CeO_2 and CeO_2-SiO_2 materials have been successfully prepared by a templating mechanism. SAXS and TEM measurements show a perfectly uniform hexagonal array of mesoporous channels with a mean pore diameter of 8 nm. The incorporation of Pt into the CeO_2-SiO_2 support produces highly active and selective catalysts for the chemoselective hydrogenation of an α,β-unsaturated aldehyde such as crotonaldehyde. The presence of small Pt metal particles together with the creation of special sites at the metal−support interface, as deduced by XPS and FTIR−CO, accounts for the excellent catalytic behavior observed. It is worth mentioning that this excellent catalytic behavior is maintained with time on stream during successive cycles. Thus, we can conclude that, within our knowledge, these results are the best reported up to now for the gas-phase hydrogenation of crotonaldehyde over Pt/MO_x catalysts at 303 K in fixed-bed continuous reaction systems.

JA031768X

(58) Vannice, M. A.; Sen, B. *J. Catal.* **1989**, *115*, 65.